JOURNAL OF SOLID STATE CHEMISTRY 104, 437–452 (1993)

$LaCuO_{2.5+x}$ and $YCuO_{2.5+x}$ Delafossites: Materials with Triangular $Cu^{2+\delta}$ Planes

R. J. CAVA, H. W. ZANDBERGEN,* A. P. RAMIREZ, H. TAKAGI, C. T. CHEN, J. J. KRAJEWSKI, W. F. PECK, JR., J. V. WASZCZAK, G. MEIGS, R. S. ROTH,† AND L. F. SCHNEEMEYER

AT&T Bell Laboratories, Murray Hill, New Jersey 07974

Received October 28, 1992; accepted January 21, 1993

The $YCuO_2$ and $LaCuO_2$ delafossites consist of alternating triangular planes of Ln^{3+} octahedra and $O–Cu^{1+}–O$ sticks. Here it is shown that under a limited set of conditions they may be oxidized to form new delafossite-derived phases $YCuO_{2.5+x}$, $0 \leq x \leq 0.05$, and $LaCuO_{2.5+x}$, $0.07 \leq x \leq 0.18$. Electron microscopy and powder X-ray diffraction are employed to characterize the resulting structures. Temperature-dependent resistivities and magnetic susceptibilities are reported. Characterization by soft X-ray photoabsorbtion spectroscopy, which shows them to be electronically unlike cuprates such as $La_{2-x}Sr_xCuO_4$, is also reported.

I. Introduction

The square planar CuO_2 arrays in layered copper oxides hold the as-yet-not-understood key to the occurrence of high-T_c superconductivity. In this regard, many theoretical and experimental studies have focused on the effects of hole doping on the square, spin $\frac{1}{2}$ Cu^{2+} ($3d^9$) array, which is antiferromagnetically ordered in, say, La_2CuO_4, when no holes are present, due to interplane interactions. Triangular plane lattices of spin $\frac{1}{2}$ Cu^{2+}, on the other hand, have not been studied. Such a system is expected to display novel magnetic collective phenomena arising from geometrical frustration of the antiferromagnetic bonds. Doping such a lattice with holes is of additional interest both to compare to the copper oxide superconductors and to test ideas of spin–charge dynamics in complex systems of low dimension.

Here we report the details of a study in which we have found that $YCuO_2$ and $LaCuO_2$ delafossites can accommodate excess oxygen at low temperatures and remain stable, with the Cu^{1+} normally present becoming oxidized to copper valences in excess of two. The copper–oxygen array is a triangular plane lattice. In the $LaCuO_{2+x}$ case, the maximum formal oxidation state of Cu is $2\frac{1}{3}$, resulting in one hole per three lattice sites. Previous studies of $LnCuO_2$ delafossites showed the effects of frustration of the magnetic moments on triangular Ln lattice (Cu^{1+} is $3d^{10}$ and nonmagnetic) as a lowering of the collective ordering temperature to well below the Curie–Weiss constant (I). This report highlights the synthesis and structural characterization of the new $YCuO_{2.5+x}$ and $LaCuO_{2.5+x}$ phases; physical properties, briefly described here, will be treated in more detail elsewhere.

The delafossite ($CuFeO_2$) crystal structure is known for a variety of transition metal oxides. The basic formula is

* National Center for High Resolution Electron Microscopy, Technical University, Delft, The Netherlands.

† National Institute of Standards and Technology, Gaithersburg, Maryland. 20899

0022-4596/93 $5.00

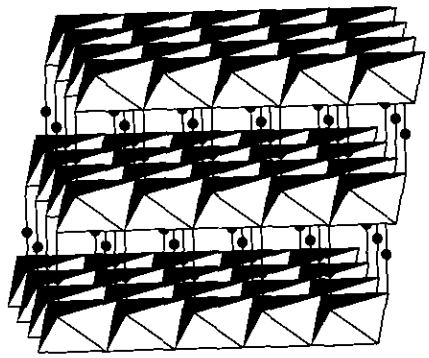

FIG. 1. The layered crystal structure of 3*R* $LaCuO_2$, showing LaO_6 octahedra and O–Cu–O sticks.

$A^{1+}B^{3+}O_2$, with A^{1+} in a linear stick coordination with oxygen, and B^{3+} in octahedral coordination (see, for instance, *2–7*). The crystal structure is shown in two projections in Figs. 1 and 2 for the example of $LaCuO_2$. The LaO_6 octahedra share edges to form a triangular plane analogous to what is observed in octahedrally coordinated transition metal dichalcogenides (such as TiS_2) with the CdI_2 structure. The oxygens on the surface of this plane serve as the coordinating atoms for the planes of Cu^{1+} atoms, which alternate with the planes of LaO_6 octahedra. The elementary structural unit is the [(LaO_2)–Cu–] double layer, which has a dimension perpendicular to the plane of 5–6 Å. The manner in which these double layers are stacked (there are several choices of O at the bottom of one double layer for Cu at the top of the neighboring double layer to bond to) is different in different materials, giving rise to a variety of delafossite polytypes. $LaCuO_2$, for instance (*5*), has the 3*R* polytype in which three double layers are stacked before the pattern is repeated. The cell is rhombohedral, $R\bar{3}m$, $a = 3.83$, $c = 17.10$ Å ($\cong 3 \times 6$). Many compounds show the 2*H* polytype, which has been reported for $YCuO_2$ (*6*). There are then two elementary double layers per cell, with symmetry $P6_3/mmc$, and, for instance $a = 3.52$, $c = 11.42$ ($\cong 2 \times 6$) for $YCuO_2$. Higher polytypes such as 6*H* have been reported (*6*). Neighboring Cu layers are separated by 5–6 Å along *c* and are always staggered such that the Cu next layer neighbors are never directly above or below.

No delafossites were previously known to allow intercalation of oxygen. For delafossites of the type ABO_2, where both *A* and *B* are transition metals, the A^{1+} inplane separation is 3 Å or less, too small to allow oxygen insertion. For $YCuO_2$ and $LaCuO_2$, however, the $a = 3.52$ and $a = 3.83$ dimensions suggest that the Cu^{1+} plane is very similar to that known to intercalate oxygen, say in $Ba_2YCu_3O_6$, except with a different geometry (Fig. 2). The Cu^{1+} plane in $LaCuO_2$, for instance, is a triangular lattice with Cu–Cu separation of 3.82 Å, compared with the Cu^{1+} plane in $Ba_2YCu_3O_6$, which is a square lattice with Cu–Cu separation of 3.86 Å. For both Y–Cu–O and La–Cu–O, however, stable compounds for Cu^{2+} are known ($Y_2Cu_2O_5$ and $La_2Cu_2O_5$), suggesting that oxidation of the delafossites without decomposition to the stable phases might be successful only at low temperatures.

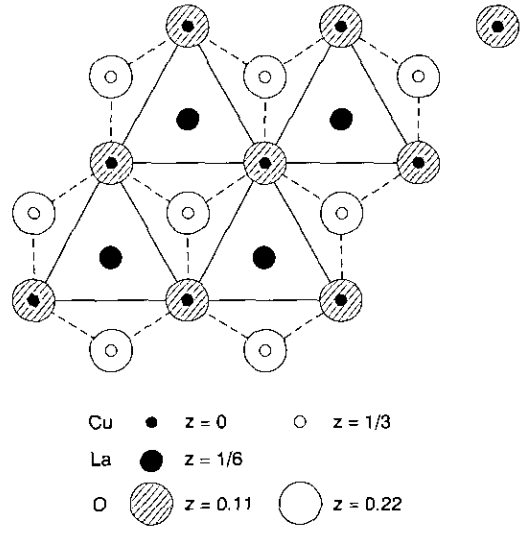

FIG. 2. A partial projection of the $LaCuO_2$ structure into the hexagonal plane. Shown are one layer of LaO_6 octahedra with triangular copper layers in the plane above (small black circles) and the plane below (small open circles). Note that the triangular Cu positions are not in registry from one layer to the next.

II. Synthesis

a. $YCuO_2$, $LaCuO_2$, and $Y_{1-x}Ca_xCuO_2$

Synthesis of polycrystalline single phase $YCuO_2$ was relatively straightforward, but different conditions yielded materials of different structural quality. As a common first step, $Y_2Cu_2O_5$ was synthesized from Y_2O_3 + CuO, fired in air at 1000 and 1100°C for several days with intermediate grindings. Reaction was continued until the product was perfect single phase $Y_2Cu_2O_5$ by powder X-ray diffraction. Samples were pressed into pellets for the final air firing step. These fired pellets were then inserted into a cold standard ceramic tube furnace and heated under flowing N_2 (60 ppm O_2 200 cm^3/min) at 1125°C for 16 hr. Samples were heated and cooled to room temperature in the gas stream. This reproducibly yielded $YCuO_2$. Both powder X-ray diffraction and electron microscopy of this product showed it to be a highly defective microscopic mixture of the delafossite polytypes 2*H*, 3*R*, and 6*H*. Excellent quality 2*H* polytype material could be obtained by a slightly different route: the single phase $Y_2Cu_2O_5$ pellets were buried in powder of the same composition, put in Al_2O_3 crucibles, and annealed at 1075°C in flowing N_2 for 40 hr (heating and cooling in the N_2 stream). A thin layer of Y_2O_3 often formed on the pellets, which was removed by sandpapering. To obtain high-purity powdered 2*H* $YCuO_2$, 2.5% excess CuO is included in the original $Y_2Cu_2O_5$ preparation. The 1075°C, 40 hr N_2 treatment is executed as described, and the resulting pellets are then pulverized and washed in stirred NH_4OH overnight at ambient temperature, dissolving any unreacted or excess Cu_2O. The oxygen content for both preparation methods was found to be 2.00/F.U. (formula unit) by measuring the weight loss incurred on reductive decomposition to Y_2O_3 + 2Cu (metal) in flowing 85% N_2–15% H_2 in a commercial TGA.

Synthesis of single-phase $LaCuO_2$ was considerably more difficult. We could not find conditions under which a single-phase $La_2Cu_2O_5$ precursor could be reduced directly to $LaCuO_2$. Of the many methods tried, only the following route yielded high-quality single-phase $LaCuO_2$ reproducibly. Freshly dried La_2O_3 (1000°C, air, 1 hr) was mixed with Cu_2O (commercial, analyzed for O : Cu ratio) stoichiometrically in 12-g batches and ground mechanically for 1 hr under N_2. Three $\frac{1}{4}$-in. thick $\frac{1}{2}$-in.-diameter pellets were pressed and buried in the remaining powder in a high-density Al_2O_3 cylinder of $\frac{5}{8}$ in. diameter and covered. That cylinder was then placed insider a larger uncovered Al_2O_3 crucible in which four 1 × $\frac{1}{2}$-in. strips of Zr foil were placed. Two of these batches were fired simultaneously in a single ceramic tube furnace (3 in. diameter, 36 in. long) under flowing N_2 (200 cm^3/min). All this trouble was *necessary* to prevent even trace amounts of O_2 from getting to the sample pellets, which resulted in the formation of La_2CuO_4 impurity. Samples were slowly heated (100°/hr) to 1000°C, left for 32 hr, and then cooled to room temperature under N_2 before being removed. Oxygen content of the single phase $LaCuO_2$ ceramic pellets was found to be 2.00/F.U. by measuring the weight loss incurred on reductive decomposition to La_2O_3 + 2Cu (metal) in flowing 85% N_2–15% H_2 in a commercial TGA.

One method that might be expected to succeed in doping $YCuO_{2+x}$ with holes is a partial substitution of Ca^{2+} for Y^{3+}, as commonly is done for superconducting copper oxides. We did in fact succeed in synthesizing delafossites $Y_{1-x}Ca_xCuO_2$ for $x \leq 0.10$ by a method similar to that employed to synthesize $YCuO_2$. First, $Y_{2-2x}Ca_{2x}Cu_2O_5$ was synthesized from Y_2O_3, $CaCO_3$, and CuO by heating in air at 1000 and 1100°C, again with the final air firing in pellet form ($x = 0.05$ is single phase, but for $x = 0.10$ the precursor is multiphase). These pellets were then fired in flowing N_2 in the ceramic tube furnace for a period of 48 hr and cooled in the N_2 flow to room temperature before removal. Firing temperatures between 975 and 1025°C

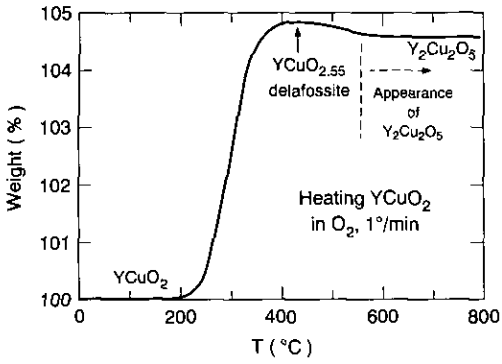

FIG. 3. Change in weight of a polycrystalline pellet of $YCuO_2$ in a commercial TGA on heating in O_2 at 1°/min to 800°C. The delafossite crystal structure is maintained to approximately 550°C.

were successful in synthesis of single-phase material. The oxygen content of $Y_{0.95}Ca_{0.05}CuO_{2+\delta}$ measured by the decomposition method was 2.05 per formula unit. We could find no synthetic conditions by which even 5% of the La in $LaCuO_2$ could be replaced by Ca or Sr.

b. Oxidation of $YCuO_2$ and $Y_{1-x}Ca_xCuO_2$

When $YCuO_2$ is heated slowly at low temperatures in O_2 it gains weight dramatically, beginning at about 200°C and reaching a maximum weight at approximately 425–450°C, as shown in Fig. 3. On heating to temperatures of 550°C and above some weight is lost. X-ray diffraction indicates the disappearance of the delafossite phase for oxygen treatments above approximately 550°C and the formation of the stable phase $Y_2Cu_2O_5$. At a temperature of 450°C the delafossite structure is maintained, with a greatly increased oxygen content, at $YCuO_{2.55}$. The formal valence of copper has increased from 1^+ to 2.1^+. Overnight heating of polycrystalline pellets of $YCuO_2$ in O_2 at temperatures of 450°C reproducibly yields final stoichiometries of $YCuO_{2.55}$ (± 0.01) and single-phase delafossite structure material. The structural changes which occur during oxidation are described in a subsequent section.

Similar results are obtained for the Ca doped material, shown, for example, in Fig. 4 for $Y_{0.95}Ca_{0.05}CuO_{2.05}$. Oxygen uptake does not become rapid until 400°C (perhaps due to pellet density), and a constant oxygen stoichiometry plateau is reached between 500 and 600°C. The oxygen content in this case reaches a maximum of 2.50/F.U., yielding a formal oxidation of Cu^{1+} to $Cu^{2.05+}$. Overnight heating of polycrystalline pellets of $Y_{0.95}Ca_{0.05}CuO_{2.05}$ in O_2 at 500°C reproducibly yields final stoichiometries of 2.50 oxygen per formula unit and single-phase delafossite structure-type material. Oxidation of $Y_{0.9}Ca_{0.1}CuO_2$ in the same manner yielded $Y_{0.9}Ca_{0.1}CuO_{2.45}$.

c. Oxidation of $LaCuO_2$

Oxidation of the $LaCuO_2$ delafossite is similar to that of $YCuO_2$ but is more complicated. Representative data for a polycrystalline pellet heated in O_2 in a commercial TGA at 1°/min to 1000°C are shown in Fig. 5. The onset of rapid weight gain is 300°C. On continued heating, the weight gain continues at a slower rate until a temperature of approximately 500°C is reached where a series of weight losses occurs on heating to higher temperatures. By 800°C, X-ray diffraction and TGA results show that the phases present are La_2CuO_4 + CuO. At the maximum weight an oxygen stoichiometry

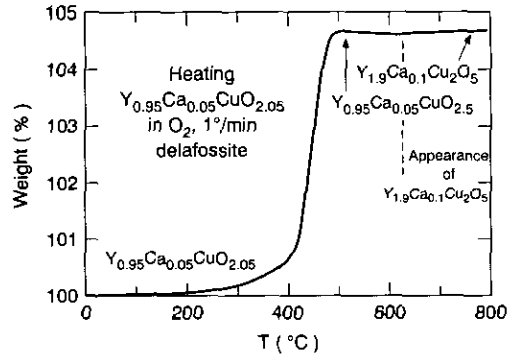

FIG. 4. Change in weight of a polycrystalline piece of $Y_{0.95}Ca_{0.05}CuO_{2.05}$ in a commercial TGA on heating in O_2 at 1°/min to 800°C. The delafossite crystal structure is maintained to approximately 600°C.

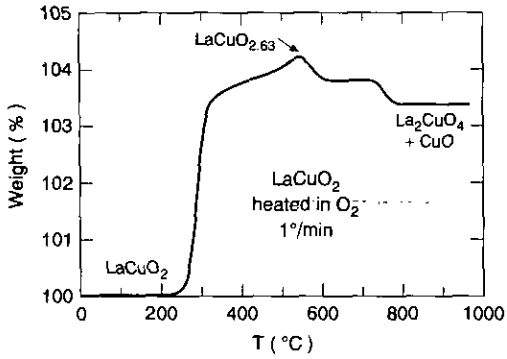

FIG. 5. Change in weight of a polycrystalline piece of $LaCuO_2$ in a commercial TGA on heating in O_2 at 1°/min to 1000°C.

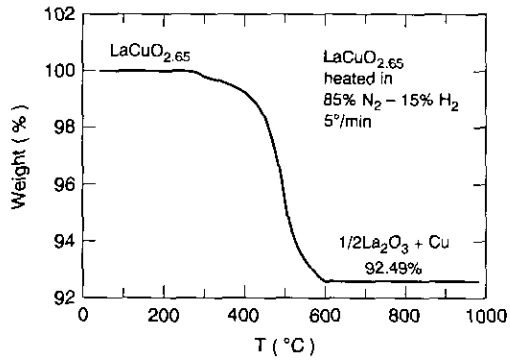

FIG. 7. Weight loss of $LaCuO_{2.65}$ delafossite (made by heating $LaCuO_2$ at 450°C in O_2 for 16 hr) on heating in a mixture of 85% N_2 15% H_2 at 5°/min. Decomposition to La_2O_3 + Cu allows determination of oxygen content of original material at 2.65/F.U.

of $LaCuO_{2.63}$ (±0.01) is obtained, yielding considerably higher formal copper valence than is possible in the $YCuO_2$ oxidation.

Due to the complex oxidation and reduction suggested by Fig. 5, further oxidation experiments were performed on $LaCuO_2$. Pieces of a polycrystalline pellet were heated at a fixed temperature for 16 hr in O_2 at temperatures between 450 and 660°C. Weight change was measured to determine the oxygen stoichiometry, and powder X-ray diffraction was employed to determine the phase assemblages. The results are summarized in Fig. 6. Delafossite structure material near stoichiometry $LaCuO_{2.66}$ is obtained at temperatures 450–475°C. At 475°C the diffraction pattern begins to show broadening of the peaks, suggesting the beginning of decomposition. At 500°C the delafossite related phase has clearly decomposed and other phases of poor crystallinity are present, which we could not identify. By 525°C the phase assemblage appears to be dominated by an $La_2CuO_{4+\delta}$ related phase which at first is poorly crystallized but becomes well formed by 650°C. The implied composition of this phase at 650°C is $La_2CuO_{4.08}$, and it is mixed with CuO. This oxygen excess 2:1 phase then decomposes to La_2CuO_4 at approximately 725°C, as shown in Fig. 5. Based on these results, the optimal oxidation temperature for $LaCuO_2$ for obtaining the oxidized delafossite phase is 450°C, yielding stoichiometries of $LaCuO_{2.66}$ (±0.01) in 16-hr treatments. Copper has been formally oxidized from 1^+ to 2.32^+.

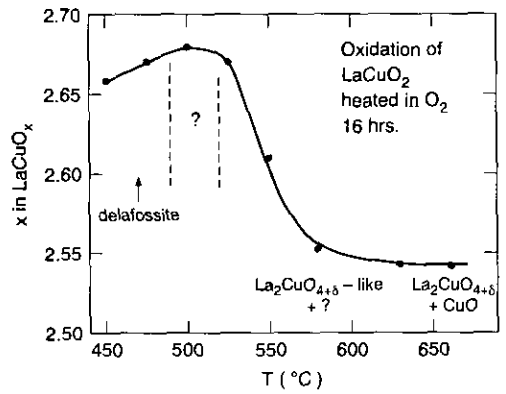

FIG. 6. Oxidation of $LaCuO_2$ heated isothermally in O_2 for 16 hr. X-ray diffraction results on products also shown.

As is commonly done for superconducting copper oxides, oxygen content of the oxidized delafossites can be measured by reductive decomposition on heating in an H_2/N_2 mixture. Representative results for a sample of $LaCuO_2$ which had been heated for 16 hr in O_2 at 450°C are shown in Fig. 7. Decomposition to $\frac{1}{2}$ La_2O_3 + Cu allows determination of the oxygen content in the original single-phase delafossite to be

$LaCuO_{2.65}$ (±0.01 O/F.U.). Note the beginning of the weight loss is at very low temperatures, 300–400°C.

Finally, we attempted to increase the oxygen content of $LaCuO_{2.66}$ prepared in O_2 at 450°C to higher values by heating at higher oxygen pressure. Heating at 400°C in 30 atm O_2 pressure for 16 hr resulted in an oxygen uptake of only 0.02 (±0.01) O/F.U. The powder X-ray diffraction lines were sharpened, suggesting improved oxygen homogeneity over the 1 atm O_2 treatment.

d. Oxygen Removal from $YCuO_{2.55}$

Oxidation of $YCuO_2$ overnight at temperatures of 500°C and below always yielded final oxygen contents greater than 2.50, therefore yielding formal copper valences in excess of 2.0^+. In order to study the physical properties of the spin ½ triangular lattice, a Cu valence of 2.00 is needed (oxygen content 2.50 per formula unit) and so we devised a method for removal of oxygen from $YCuO_{2.55}$. The method employed was Zr-gettered annealing, which has yielded high-quality samples of $Ba_2YCu_3O_{7-x}$ (*8*). In this method, small pieces of polycrystalline pellets of $YCuO_{2.55}$ were placed in a sealed evacuated quartz tube with different amounts of Zr foil and heated isothermally. It was found that an annealing temperature of 440°C for a period of 3 nights gave satisfactory results. The oxygen content of the final product is determined by careful measurement of the weight loss (±.00001 g) after treatment. Results from one particular annealing run are presented in Table 1. For the present materials, general reproducibility of oxygen content from run to run under the same conditions was ±0.01 O/F.U. Reproducible behavior depends on factors such as Zr foil cleanliness and placement (a 1-in. quartz spacer was used to prevent Zr–sample contact), pellet porosity, and thermal gradients in the annealing furnace.

For both the La and Y delafossites, there are large changes in crystallographic cell volume in oxidation. It therefore is not clear whether $LnCuO_{2+x}$ will be a solid solution for all x or will be a two-phase mixture at intermediate x values. Powder X-ray diffraction measurements of the Zr-gettered samples showed the existence of two distinct phases for $YCuO_{2+x}$ for $0 < x < 2.50$. The oxidized delafossite was only single phase between $YCuO_{2.50}$–$YCuO_{2.55}$. At lower total oxygen content, e.g., $YCuO_{2.45}$, materials were a mixture of $YCuO_{2.50}$ and $YCuO_{2.00}$, with $YCuO_{2.00}$ increasing in proportion as the total oxygen content decreased toward two.

TABLE I

OXYGEN REMOVAL FROM $YCuO_{2.55}$ AND $LaCuO_{2.64}$ BY Zr-GETTERED ANNEALING

No. Zr	Sample weight (g)	Final $YCuO_x$	X ray
a. $YCuO_{2.55}$ from 500°C O_2 oxidation			
0	0.35	2.54	Single phase
½	0.24	2.51	Single phase
1	0.24	2.45	2.50 + 2.00
2	0.24	2.37	2.50 + 2.00
3	0.24	2.30	2.50 + 2.00
Anneal: 440°C, 3 nights			
b. $LaCuO_{2.64}$ from 425°C O_2 oxidation			
3	.87	2.59	Single phase
5	.91	2.57	Single phase
7	.97	2.56	Single phase
10	.98	2.52	Single phase?
13	1.01	2.48	Decomposition
16	1.09	2.47	Decomposition
Anneal: 420°C, overnight			

Note. Size of Zr strips: ½ in. × 1½ in. size of evacuated quartz tubes: 10 mm ID, 6 in. length.

e. Oxygen Removal from $LaCuO_{2.64}$

As for $YCuO_2$, oxidation of $LaCuO_2$ always yielded oxygen contents in excess of 2.50 per formula unit and therefore resulted in formal copper valences greater than Cu^{2+}. Oxidation of $LaCuO_2$ at temperatures between 425 and 450°C in O_2 overnight yielded oxygen contents between $LaCuO_{2.64}$–$LaCuO_{2.66}$. Removal of oxygen from this phase was a considerably more delicate process than for $YCuO_{2.55}$ as it is

much less stable under all conditions than its Y counterpart. To avoid decomposition on oxygen removal, the Zr-gettered annealing had to be performed at lower temperatures and for shorter times than for $YCuO_{2.55}$. Satisfactory results were obtained at 400–420°C in overnight treatments. Higher temperatures resulted in decomposition, and at lower temperatures the Zr foil was not active enough to remove oxygen from the samples. Results from one oxygen removal run are presented in Table I, for starting material of composition $LaCuO_{2.64}$. Again, reproducibility from run to run is ± 0.01 oxygen per formula unit.

Determination of the oxygen-content stability of oxidized $LaCuO_{2+x}$ delafossite was not as straightforward as in the $YCuO_{2+x}$ case. At total oxygen contents of 2.48 and below, the delafossite phase is decomposed under our gettering conditions: 3*R* $LaCuO_2$ is not the phase that grows in for oxygen contents decreasing toward 2.0 per formula unit. Although that is clear in the powder diffraction, at intermediate oxygen contents, $LaCuO_{2.55}$–$LaCuO_{2.50}$, there may be a poorly crystallized or amorphous phase present which contributes only to the background of the powder diffraction pattern. Including the data from the 30 atm O_2 treatment, the oxidized $LaCuO_{2+x}$ delafossite appears to exist as single-phase material from $LaCuO_{2.68}$ down to approximately $LaCuO_{2.57}$. The lower oxygen content limit must be regarded as tentative, but this conclusion is consistent with magnetic and spectroscopic results to be reported in a subsequent section. If the minimum oxygen content is indeed 2.57, then the $LaCuO_{2+x}$ delafossite cannot be reduced to a state which allows the study of Cu^{2+} in a triangular lattice of equivalent dimension to that of square-lattice copper oxides.

III. Structural Characterization

a. Electron Microscopy

Thin specimens for electron microscopy were obtained by crushing polycrystalline pellets and mounting the crystal fragments on a Cu grid covered with a carbon coated holey film. Electron microscopy was performed with a Phillips CM30ST electron microscope operating at 300 kV and equipped with a side-entry 25°/25° tilt specimen holder. Electron diffraction and high-resolution electron microscopy (HREM) were carried out with a number of crystallites of several batches of the compositions $YCuO_2$, $Y_{0.95}Ca_{0.05}CuO_2$; $LaCuO_2$, $YCuO_{2.51}$, $YCuO_{2.57}$, $LaCuO_{2.65}$; and $Y_{0.95}Ca_{0.05}CuO_{2.5}$.

Electron diffraction showed that the unit cells of the compounds $YCuO_2$, $Y_{0.95}Ca_{0.05}CuO_2$, and $LaCuO_2$ were all hexagonal with an *a* axis of approximately 3.5–3.8 Å, but the *c* axis was observed to be variable in length, indicating a variation in the stacking along the *c* axis, e.g., the mixing of different polytypes. This stacking, especially for $YCuO_2$, was found to vary from sample to sample, and even from crystal fragment to crystal fragment within one batch. The density of stacking defects was compatible with the results obtained from X-ray powder diffraction: in the cases where a batch showed a clear single phase diffraction pattern the amount of other types of stacking present was found to be relatively small.

All the oxidized delafossites were found to have superstructures. $YCuO_{2.55}$ adopts an orthorhombic $2a,a\sqrt{3},c$ superstructure. $YCuO_{2.51}$ shows a more complicated diffraction pattern, which indicates a mixture of $2a,a\sqrt{3},c$ and $a\sqrt{3},a\sqrt{3},c$ superstructures and regions having no superstructure. In Fig. 8b the $[010]_s$ of $YCuO_{2.55}$ is shown, which should be compared with the $[-110]_b$ diffraction pattern of the basic structure (Fig. 8a). The $[010]_s$ diffraction pattern has systematic absences for $h0l$: $4 + l \neq 2n$. The reflections with $h = 2n$ are all sharp but the reflections with $h \neq 2n$ are elongated along c^*. In some crystallites rather weak extra spots were visible corresponding to the diffraction pattern of an $a\sqrt{3},a\sqrt{3},c$ superstructure, but in all investigated crystallites the intensities of the $2a,a\sqrt{3},c$ super-

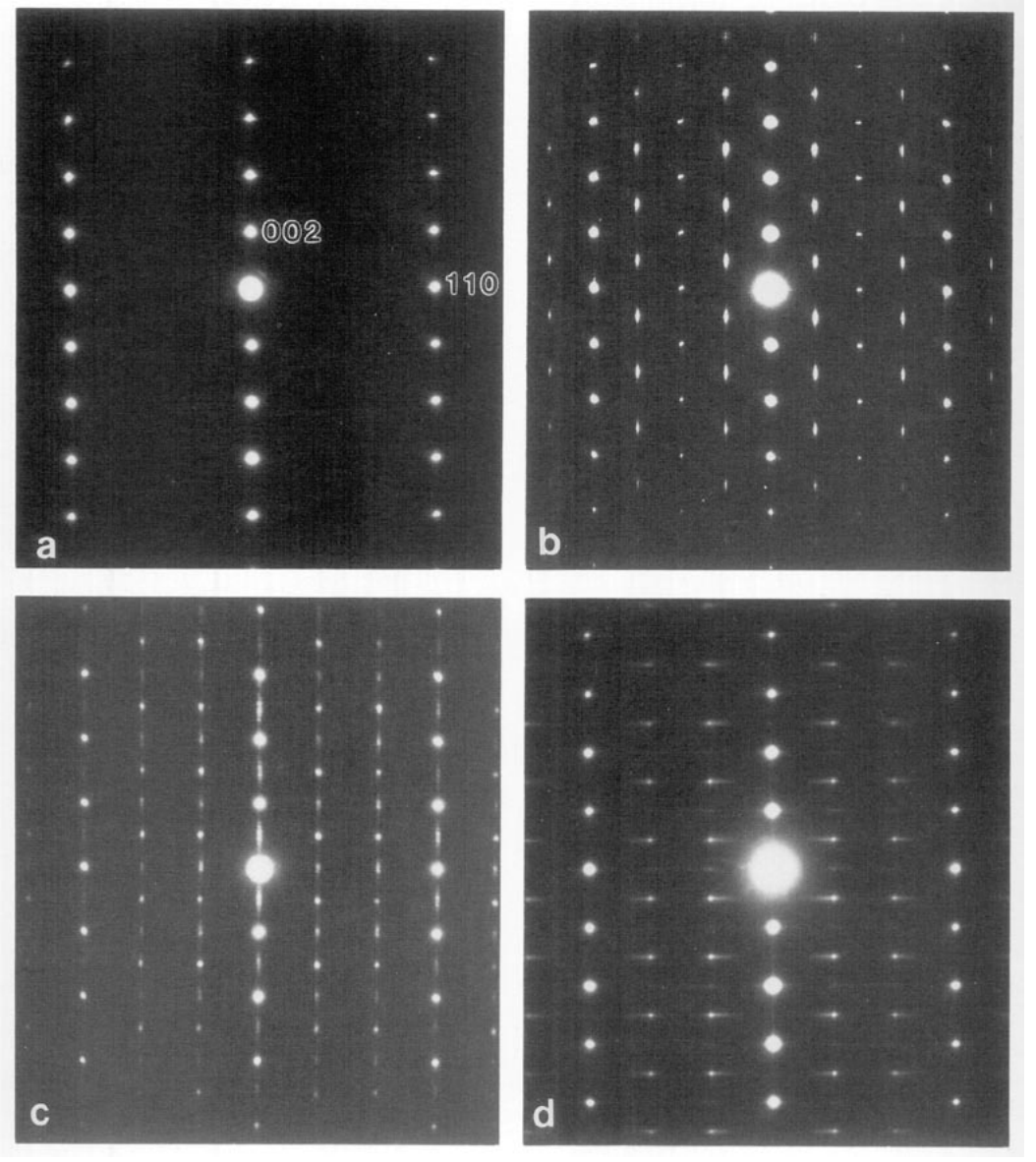

FIG. 8. Electron diffraction patterns of (a) $YCuO_2$, (b) $YCuO_{2.55}$, (c) $LaCuO_{2.65}$ and (d) $Y_{0.95}Ca_{0.05}CuO_{2.5}$. $YCuO_2$ like $Y_{0.95}Ca_{0.05}CuO_2$ and $LaCuO_2$ shows no superstructure, whereas all oxidized compounds adopt superstructures. $YCuO_{2.55}$ adopts an orthorhombic unit cell of $2a,a\sqrt{3},c$. $Y_{0.95}Ca_{0.05}CuO_{2.5}$ and $LaCuO_{2.65}$ have an $a\sqrt{3},a\sqrt{3},c$ superstructure. Not all superstructure reflections are sharp, as can be seen from (b), (c), and (d).

structure were much stronger. $LaCuO_{2.65}$ and $Y_{0.95}Ca_{0.05}CuO_{2.5}$ have, in the first approximation, a similar type of superstructure: $a\sqrt{3},a\sqrt{3},c$, as can be seen from Figs. 8c and 8d, but they differ in symmetry and in diffuse scattering. Figures 8c and 8d show the $[-120]_s$ diffraction pattern which can be compared with the $[-110]_b$ diffraction pattern of the basic unit cell (Fig. 8a). La $CuO_{2.65}$ has systematic absences for $h0l$ with

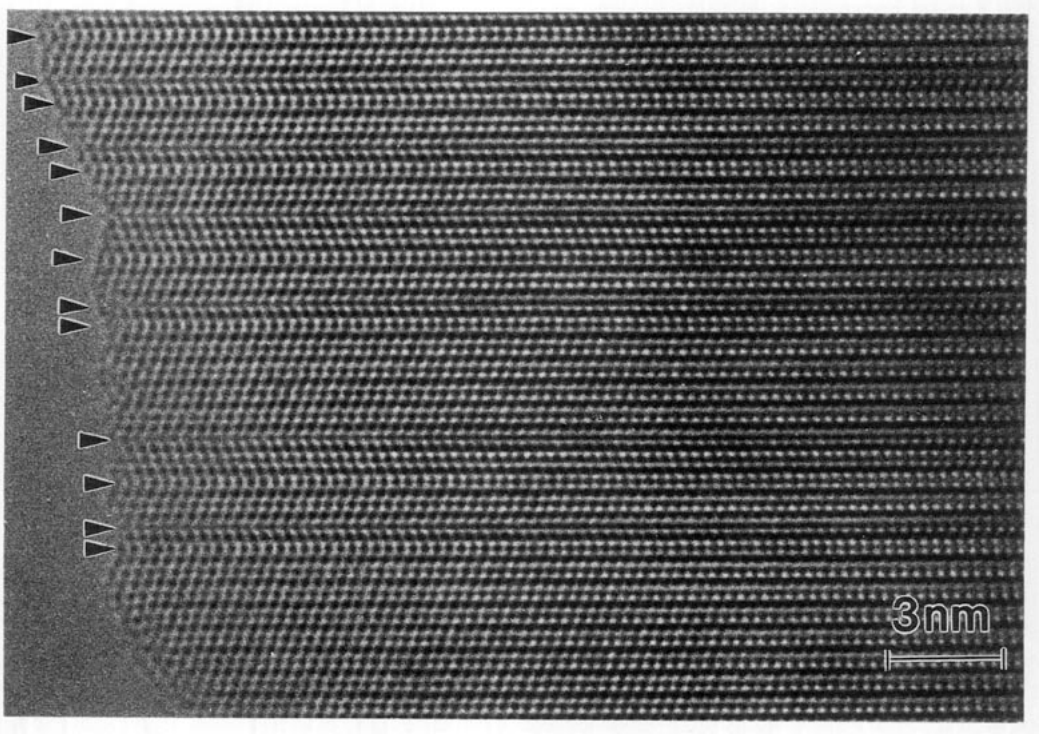

FIG. 9. [010] high-resolution micrograph of $YCuO_2$ (prepared at 1125°C for 16 hr in N_2) showing a typical example of the variation in the stacking which can be observed in specimens which have a complex X-ray diffraction pattern. Deviations from a cubic stacking along the c axis (running in perpendicular direction) are indicated by arrows. Y and Cu atoms are imaged as black dots in the thin part of the crystal (left).

$l \neq 2n$ if $h = 3n$ and $l = 2n$ if $h \neq 3n$ for the sharp reflections whereas these conditions are reverse for the reflections which are streaked along c^*. Taking the same basic unit cell, the systematic absences for $Y_{0.95}Ca_{0.05}CuO_{2.5}$ are $h0l$ with $l \neq 2n$ if $h = 3n$ and $l = 2n$ if $h \neq 3n$ for the sharp reflections. Streaking occurs along the $[100]_s$ direction and alternatingly away and toward the row $h0l$ with $h = 3n$ for $l = 2n$ and $l \neq 2n$ respectively.

HREM was carried out on the same samples investigated by electron diffraction. The fraction of stacking defects observed was in agreement with the intensity of the streaking in the electron diffraction patterns. Figure 9 shows an example of the large fraction of stacking defects which can occur, taken from a sample of $YCuO_2$ synthesized at 1125°C in N_2 for 16 hr. Regions of $2H$, $3R$, and $6H$ stacking are seen. The fraction and type of stacking defect present is dependent on both the composition and synthetic conditions of the delafossite phase. A more extensive HREM investigation will be published elsewhere.

b. Powder X-ray Diffraction

Samples of the reduced and oxidized delafossites were analyzed by conventional powder X-ray diffraction ($CuK\alpha$ radiation, θ–2θ scans). Powder X-ray patterns for $3R$ $LaCuO_2$, $a = 3.83$ $c = 17.10$, and $2H$ $Y_{0.95}Ca_{0.05}CuO_{2.05}$, $a = 3.525$, $c = 11.43$, are shown in Figs. 10 and 11. The pattern (and cell parameters) for pure $2H$ $YCuO_{2.00}$, when prepared as described, are virtually identical to that of $Y_{0.95}Ca_{0.05}CuO_{2.05}$ and so

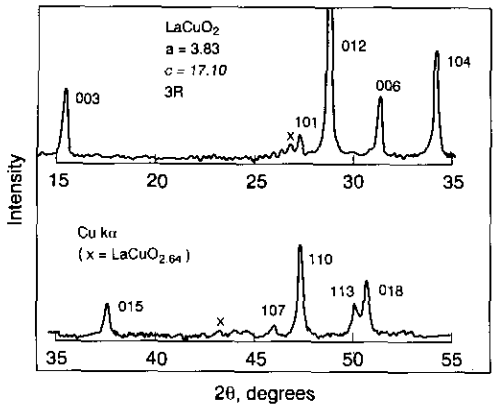

FIG. 10. Powder X-ray diffraction pattern for 3*R* $LaCuO_2$.

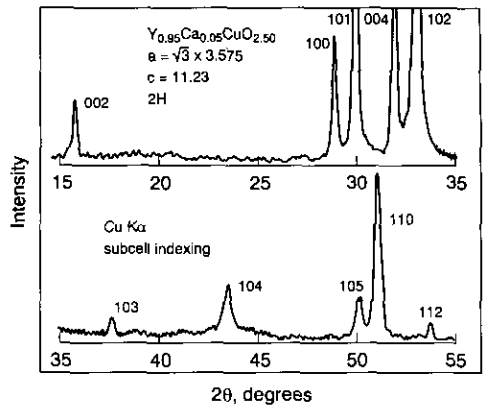

FIG. 12. Powder X-ray diffraction pattern for the oxidized delafossite $Y_{0.95}Ca_{0.05}CuO_{2.50}$.

are not shown. The unit cell parameters are in excellent agreement with those in the literature. For $LaCuO_2$, small peaks (marked with an x in Fig. 10) are often observed corresponding to the strongest peaks in the oxidized delafossite $LaCuO_{2.65}$: the oxidized phase occurs on the surface of the pellets. Note that reflections $Y_{0.95}Ca_{0.05}CuO_{2.05}$ have different widths dependent on their index. This is due to the fact that the stacking faults of different polytypes affect the peak widths differently: in general the 10*l* reflections are the broadest. For samples of $YCuO_2$ in which significant regions of 3*R* stacking are observed in the TEM (see Fig. 9), a strong, broad, 3*R* 102 reflection is observed in the powder X-ray pattern, with $c \cong \frac{3}{2} * 11.43$.

Powder X-ray diffraction patterns for three oxidized delafossites are shown in Figs. 12, 13, and 14. For $Y_{0.95}Ca_{0.05}CuO_{2.50}$ electron microscopy shows very good 2*H* stacking with a $\sqrt{3}$ superlattice in the basal plane such that the true cell is hexagonal with $a' = \sqrt{3} \cdot 3.575$, $c = 11.23$. Figure 12 shows the good crystalline quality of the oxidized phase and also that none of the superlattice peaks due to oxygen ordering are visible in the general X-ray scan. For

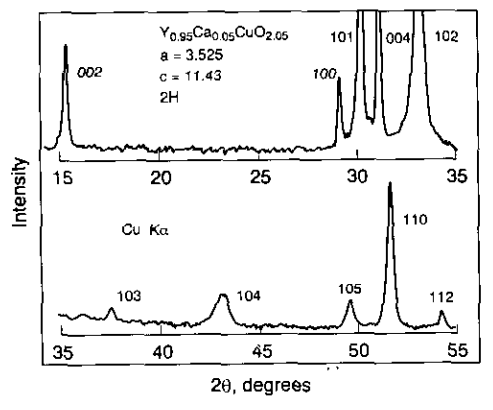

FIG. 11. Powder X-ray diffraction pattern for 2*H* $Y_{0.95}Ca_{0.05}CuO_{2.05}$; the pattern for 2*H* $YCuO_2$ is virtually identical to this one.

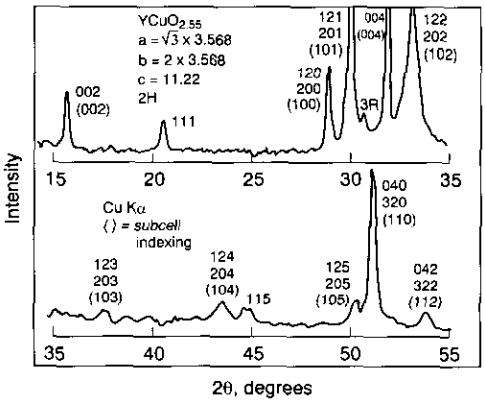

FIG. 13. Powder X-ray diffraction pattern for the oxidized delafossite $YCuO_{2.55}$. The peak marked 3*R* is the strongest peak of the 3*R* polytype.

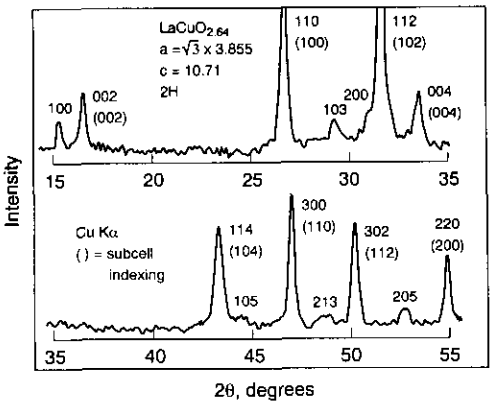

FIG. 14. Powder X-ray diffraction pattern for the oxidized delafossite $LaCuO_{2.64}$.

$YCuO_{2.55}$, electron microscopy again shows good $2H$ stacking, but now shows an orthorhombic distortion of the supercell: with $b' = 2a = 7.14$, $a' = \sqrt{3}a = 6.18$ in the basal plane ($a = 3.568$) and $c' = c = 1.22$ estimated from the powder X-ray diffraction pattern. A few superlattice peaks are visible in the general X-ray scan, Fig. 13. The relatively large width of the 102 subcell reflection (compare to Fig. 12) shows the presence of stacking faults in $YCuO_{2.55}$ and the small peak marked in Fig. 13 is the strongest reflection from the well-crystallized regions of $3R$ polytype.

For $LaCuO_{2.65}$, TEM shows a $2H$ stacking with a strong $\sqrt{3}a$ superlattice in the basal plane. From the powder X-ray diffraction pattern (Fig. 14) the unit-cell dimensions are estimated to be $a' = \sqrt{3} \cdot 3.855 = 6.677$, $c = 10.71$. The polytype stacking has changed from $3R$ to $2H$ during oxidation. For this material, several superlattice peaks are easily visible in the general powder X-ray scan. Note, surprisingly, that the c-axis length for $2H$ $LaCuO_{2.65}$, 10.71 Å, is considerably shorter than that for $2H$ $YCuO_{2.55}$, 11.22 Å, in spite of the larger size of the La–O octahedron. This suggests that the distribution of the copper and intercalated oxygen in the Cu planes is considerably different in the two materials. Note also the small c-axis shrinkage from 11.42 to 11.22 Å on oxidation of $2H$ $YCuO_{2.00}$ to $YCuO_{2.55}$, reflecting the decrease of the out-of-plane Cu–O bondlength on oxidation of Cu^{1+} to Cu^{2+}. Neutron diffraction measurements are currently underway to determine the crystal structures for the oxidized materials.

IV. Physical Property Measurements

Resistivity was measured on polycrystalline pellets of $YCuO_{2+x}$ and $LaCuO_{2+x}$ oxidized delafossites in a four-probe bar geometry. Results are shown in Fig. 15. $YCuO_{2.55}$ and $YCuO_{2.51}$ are semiconductors with room temperature resistivities of 10^2 and 10^3 ohm-cm respectively. Plotting of the data in a log ρ vs $1/T$ representation shows curvature over the entire temperature range with an implied activation energy of approximately 0.23 eV for $YCuO_{2.51}$ near 300 K. The activation energy is slightly smaller for $YCuO_{2.55}$. As seen in the figure, the oxidation of Cu to 0.1 hole/Cu improves the resistivity but does not result in metallic behavior. For $LaCuO_{2+x}$, the resistivities measured are significantly lower, and increase as expected as decreasing oxygen content decreases the Cu valence toward Cu^{2+}. Note, however, that although the magnitudes of the resistivities measured are relatively high, they do not increase very

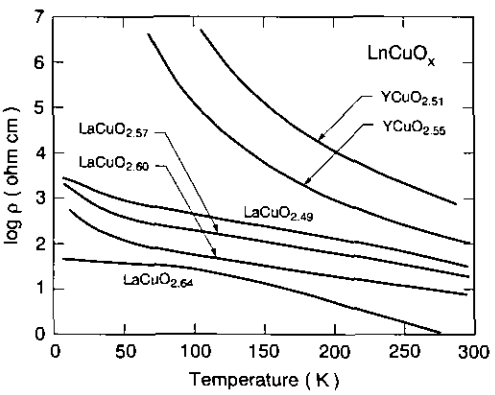

FIG. 15. Temperature dependent resistivities of polycrystalline pellets of $YCuO_{2+x}$ and $LaCuO_{2+x}$.

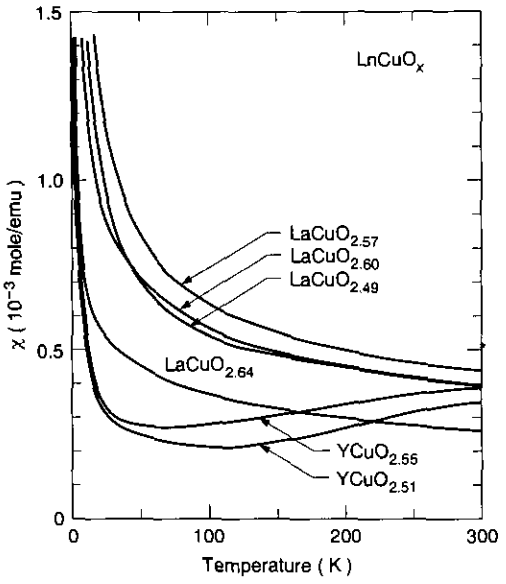

FIG. 16. Temperature dependent magnetic susceptibilities of $YCuO_{2+x}$ and $LaCuO_{2+x}$, linear scales.

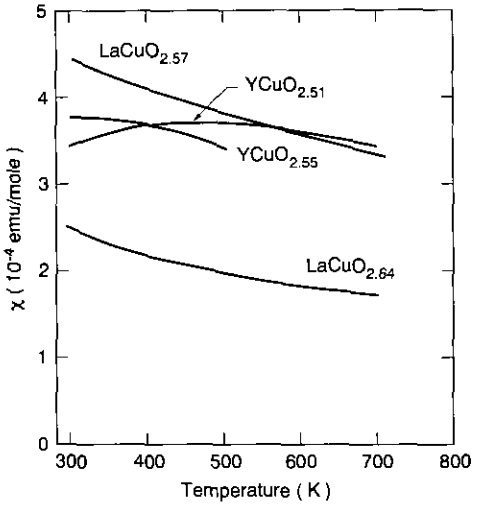

FIG. 17. Magnetic susceptibilities for selected La CuO_{2+x} and $YCuO_{2+x}$ compositions above room temperature, linear scales.

much with decreasing temperature. The observed temperature dependence is more consistent with a resistivity several orders of magnitude lower than what is measured. This suggests that in the $LaCuO_{2+x}$ case the resistivities are dominated by grain boundary resistance in these low density pellets, and that the intrinsic resistivities may be one or two orders of magnitude lower than those presented in Fig. 15.

Magnetic susceptibilities were measured for the oxidized series in a SQUID magnetometer in a field of 1 T. Results for representative samples are shown in Figs. 16–20, where a contribution for core diamagnetism has been subtracted. Both sets of materials have susceptibilities which display local moment behavior at low temperatures. For the $YCuO_{2.5+x}$ materials, the susceptibility increase at low temperatures corresponds to a moment of $0.2\mu_B$, or 5% free Cu^{2+} spins. No sign of three-dimensional magnetic ordering was observed down to 2 K. This is consistent with that expected for a frustration-dominated spin system. Also as expected, the magnitude of the susceptibilities decreases with increasing hole concentration. The susceptibilities at high temperatures, however, differ for the Y- and La-based compounds. Figure 16 shows continuously increasing susceptibilities with decreasing temperature for $LaCuO_x$, but for

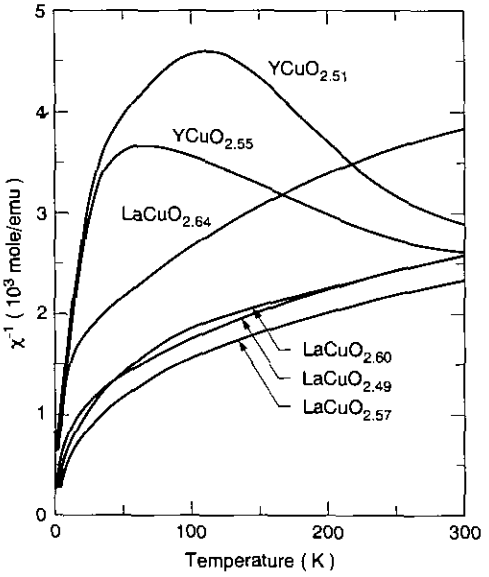

FIG. 18. Temperature dependent magnetic susceptibilities of $YCuO_{2+x}$ and $LaCuO_{2+x}$, inverse χ scale.

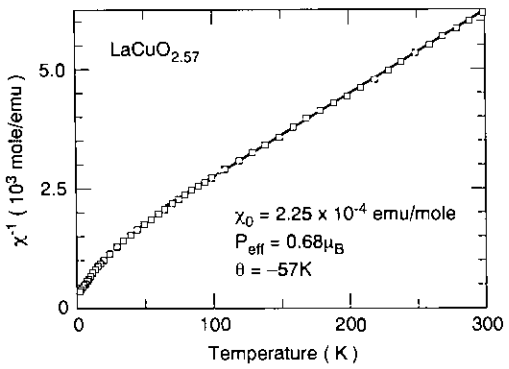

FIG. 19. Magnetic susceptibility of $LaCuO_{2.57}$ after subtraction of a temperature-independent term, showing fit to $\chi - \chi_0 = C/(T - \theta)$ between 65 and 300 K.

$YCuO_x$ the susceptibilities first decrease on cooling from 300 K. Measurements to 700 K (Figure 17) show that the decrease below 300 K is the lower part of very broad shallow peaks in the susceptibilities with maxima near 400 and 300 K for $YCuO_{2.51}$ and $YCuO_{2.55}$ respectively. $LaCuO_x$ shows no peaks or changes in curvature up to 700 K. Data in Fig. 17 are reproducible on heating and cooling over the temperature range plotted indicating stability of the phases (structure and oxygen content) up to 700 K for all except $YCuO_{2.55}$ which showed decomposition above 500 K.

In Fig. 18 the inverse susceptibilities, χ^{-1}, are shown as a function of temperature. For $YCuO_x$ the broad maxima in χ near 300 K give rise to apparent maxima in χ^{-1} at lower temperatures. For $LaCuO_x$, the susceptibilities show curvature over the whole temperature range, and if taken as is can be fit to Curie–Weiss like behavior only at temperatures in the range 200–300 K. Such a fit for $LaCuO_{2.57}$, for example, yields an effective moment $\rho_{\text{eff}} = 1.6\mu_B$, close to the spin $\frac{1}{2}$ value of $1.73\mu_B$, and a Curie–Weiss temperature $\theta_{\text{cw}} = -490$ K. Fits for other compositions yield similar results.

Although the $LaCuO_x$ compounds are not metallic conductors, they are somewhat conductive and so the χ^{-1} presented in Fig. 18 may include a temperature independent susceptibility χ_0 due to the Pauli Paramagnetism of free carriers. Assuming that to be the case, the data for $LaCuO_{2.57}$ are replotted with a χ_0 subtracted calculated from a fit to $\chi - \chi_0 = C/(T - \theta)$ in the region 65–300 K. The data are seen to be very well described above 65 K with $\theta = -57$ K, $\rho_{\text{eff}} = 0.68\mu_B$, and $\chi_0 = 2.25 \times 10^{-4}$ emu/mole, suggesting that the nonzero χ_0 term is indeed present. The deviation from Curie–Weiss behavior at low temperatures ($T < 65$ K here) is typical for geometrically frustrated systems (9) and is due to the onset of short-range spin correlations. Taking $\theta_{\text{cw}} = -57$ K at face value, and assuming the nearest neighbor inplane exchange interaction dominates the exchange energy, $E_{\text{ex}} = 2J_{\text{nm}} \cdot S_i S_j$, one finds $J_{\text{nm}} \cong 19$ K, significantly less than the $J_{\text{nm}} \cong 1500$ K in La_2CuO_4. This qualitative difference is likely due to the 180° O–Cu–O bonding in La_2CuO_4 and the probable lack of such linear bonding in the triangular Cu–O array in $LaCuO_x$.

Finally, Fig. 20 shows the oxygen stoichiometry dependence of the magnetic susceptibility at 300 K for the $LaCuO_x$ oxidized series. There is a peak at $x = 2.57$. Our present interpretation of this behavior is that above $x = 2.57$ susceptibility decreases with increasing hole concentration as expected,

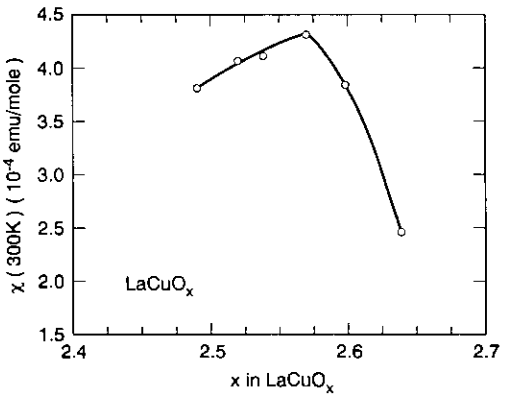

FIG. 20. Oxygen stoichiometry dependence of the 300 K magnetic susceptibility of $LaCuO_x$. The decrease below $x = 2.57$ may be due to decomposition.

but that below $x = 2.57$ there is decomposition of the oxidized delafossite under our conditions to a Cu^{1+}-containing phase which is essentially nonmagnetic. The magnetic data form a part of the evidence which leads us to conclude that there is a minimum oxygen content for the oxidized $LaCuO_x$ delafossite under our conditions of approximately $x = 2.57$.

V. Spectroscopy

To investigate the electronic structure of the conducting holes in $LaCuO_x$ and $YCuO_x$, we have measured the bulk sensitive, O K-edge and Cu $L_{2,3}$-edges photoabsorption spectra. The experiments were performed using the AT&T Bell Laboratories Dragon beamline located at the National Synchrotron Light Source, Brookhaven National Laboratory (*10*). The monochromator resolution was set at ~0.15 and ~0.45 eV for the O K-edge and Cu $L_{2,3}$-edges, respectively. Bulk-sensitive (~2000 Å probing depth) fluorescence yield spectra were recorded using a high-sensitivity seven-element germanium array detector. The sample surfaces were scraped in air immediately before pumping down the spectrometer vacuum chamber, and the measurements were carried out at room temperature.

Figure 21 shows the O K-edge (O $1s \rightarrow$ O $2p$ transitions) and Cu $L_{2,3}$-edges (Cu $2p_{1/2,3/2} \rightarrow$ Cu $3d, 4s$ transitions) fluorescence yield photoabsorption spectra of $LaCuO_2$ and $LaCuO_{2.64}$. The spectra for $YCuO_2$ and $YCuO_{2.55}$ are shown in Fig. 22. Upon oxygen doping of $LaCuO_2$ and $YCuO_2$, a new unoccupied O $2p$ band, labeled as peak O2, appears in both the O K-edge spectra of $LaCuO_{2.64}$ and $YCuO_{2.55}$. Since the intensity of peak O2 increases with oxygen content (see Figs. 23 and 24), this new unoccupied O $2p$ band is ascribed to the oxygen atoms doped into the Cu planes (denoted as "O2" oxygens). Interestingly, the double-peak feature in the lowest unoccupied band in the undoped samples, labeled as peak O1,

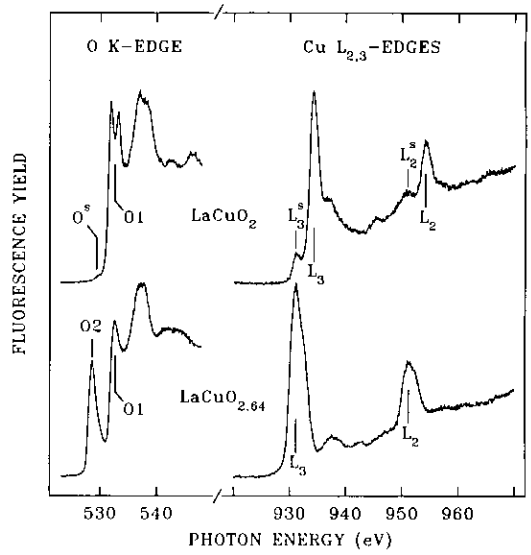

FIG. 21. O K-edge and Cu $L_{2,3}$-edges fluorescence yield photoabsorption spectra of $LaCuO_2$ and $LaCuO_{2.64}$. The peaks labeled in the figure are discussed in the text.

becomes a single-peak feature in the doped samples. This peak is ascribed to the oxygens between the La and the Cu planes (denoted as the "O1" oxygens), because its intensity (peak area) is essentially the same for both undoped and doped samples. The change in the lineshape of O1 peak could be due either to the change in the bond distance between the O1 oxygens and the Cu, or to an indirect influence on the chemical environment of the O1 oxygens by the added presence of the O2 oxygens.

Two strong absorption white lines, labeled as L_2 and L_3, were observed in the Cu $L_{2,3}$-edges spectra of all four samples. The ~3-eV shift toward the lower photon energy of the white lines of doped samples, in comparison to undoped samples, is a characteristic of the Cu^{1+} and Cu^{2+} oxidation states of Cu atoms in cuprates (*11*). This observation clearly shows that the Cu atoms are in the Cu^{1+} oxidation state in undoped samples and are in the $Cu^{2+\delta}$ oxidation state in doped samples. By normalizing these Cu $L_{2,3}$-edges spectra to make their intensities equal

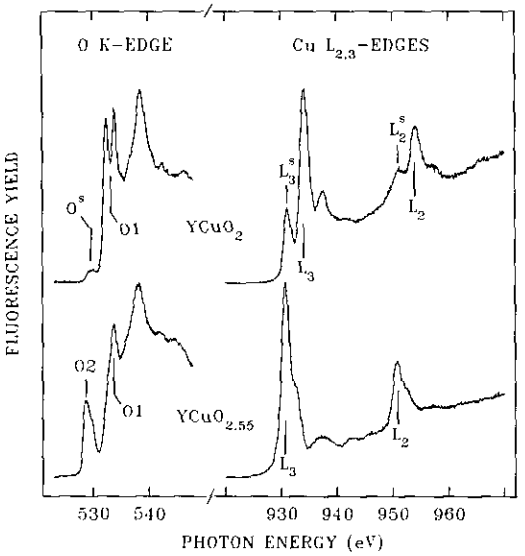

FIG. 22. O K-edge and Cu $L_{2,3}$-edges fluorescence yield photoabsorption spectra of $YCuO_2$ and $YCuO_{2.55}$. The peaks labeled in the figure are discussed in the text.

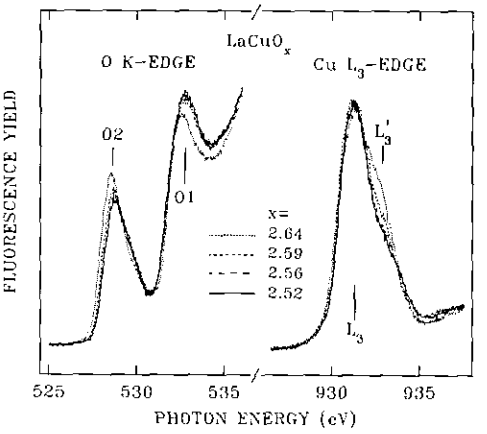

FIG. 23. The low-energy region of the O K-edge and the L_3 white line region of the Cu $L_{2,3}$-edge spectra of four different oxidized $LaCuO_x$ samples.

at 970 eV, a well-known procedure for taking into account the differences in experimental conditions, we find that the intensities of the $L_{2,3}$ white lines of the undoped samples are much smaller than those of the white lines of the doped samples. This intensity difference strongly suggests that the main photoabsorption transition for undoped samples (Cu^{1+}) is $2p^63d^{10} \rightarrow 2p^53d^{10}4s^1$, and for doped samples (Cu^{2+}) is $2p^63d^9 \rightarrow 2p^53d^{10}$, because the $2p \rightarrow 4s$ transition is known to have a much smaller absorption cross-section than that of the $2p \rightarrow 3d$ transition. The extra peaks observed in the undoped samples, labeled as L_2^s, L_3^s, and O^s, are all due to the oxidation of sample surfaces before the pumping down of the vacuum chamber. This surface oxidation effect is confirmed by the large increase in the L_2^s/L_2, L_3^s/L_3, and $O^s/O1$ ratios found in the surface sensitive (~100 Å probing depth) total electron yield spectra (not shown), recorded simultaneously with the fluorescence yield spectra. The nearly identical energy positions between the $L_{2,3}^s$ of undoped samples and the $L_{2,3}$ peaks of doped samples clearly show that the oxidized surface layers of undoped samples are in the Cu^{2+} oxidation state.

To investigate the electronic character of the conducting holes induced by oxygen doping beyond $x = 2.5$ (Cu^{2+}), Figs. 23 and 24 show the spectra of the O K-edge low-energy and the Cu L_3 white line regions for four $LaCuO_x$ and two $YCuO_x$ samples, respectively. Upon oxygen doping beyond $x = 2.5$, the intensity of peak O2 increases slightly, consistent with the further increase

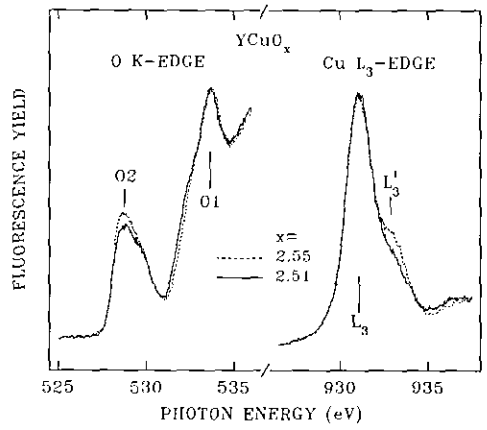

FIG. 24. The low-energy region of the O K-edge and the L_3 white line region of the Cu $L_{2,3}$-edges spectra of two different oxidized $YCuO_x$ samples.

in the total number of oxygen atoms in the Cu planes. Neither a new absorption peak, nor a large enhancement in peak O2 was observed with oxygen doping beyond $x = 2.5$. This is in clear contrast to the case of doped La_2CuO_4, in which a new intense peak appears at the lowest energy region of the O *K*-edge spectra, demonstrating that the conducting holes in $La_{2-x}Sr_xCuO_{4+\delta}$ have a strong O 2*p* character (*12*). This comparison suggests that the conducting holes in $LaCuO_{x>2.5}$ and $YCuO_{x>2.5}$ do not have a significant amount of O 2*p* character. The unoccupied band (peak O2) induced by oxygen doping behaves more like localized holes, having little contribution to conductivity. On the other hand, the shoulder of the Cu L_3 white line (labeled as L_3') exhibits more enhancement, with oxygen doping beyond $x = 2.5$, than that observed in $La_{2-x}Sr_xCuO_4$ (*13*), indicating that the conducting holes in $LaCuO_{x>2.5}$ and $YCuO_{x>2.5}$ have more Cu 3*d* character. This difference in the O 2*p* to Cu 3*d* character ratio of the conducting holes provides a possible microscopic explanation for the high resistivities of $LaCuO_{x>2.5}$ and $YCuO_{x>2.5}$ when compared to that of $La_{2-x}Sr_xCuO_4$. It is conceivable that a small O $2p_{x,y}$ to Cu 3*d* character ratio of the conducting holes could hinder the hopping between O and Cu atoms, thus giving a much lower conductivity in the Cu planes of $LaCuO_{x>2.5}$ and $YCuO_{x>2.5}$. Theoretical calculations to confirm this explanation would be of interest.

VI. Conclusion

We have shown that the $YCuO_2$ and $LaCuO_2$ delafossites can be oxidized under a limited set of conditions to form new phases with stoichiometries $YCuO_{2.5+x}$ and $LaCuO_{2.5+x}$. Oxygen can then be removed by low-temperature gettering to manipulate the formal valence of Cu in the vicinity of Cu^{2+}. The physical properties of the triangular planes of $Cu^{2+\delta}O$ present are of interest both in their own right and as a comparison to the square planes of CuO_2 in cuprate superconductors. Detailed interpretation of the magnetic properties is not yet complete, as more microscopic studies of the Cu spin state are required. Those studies, as well as structural determination by powder neutron diffraction and detailed electron microscopy investigation are in progress and will be reported elsewhere.

References

1. A. P. Ramirez, R. Jager-Waldau, and T. Siegrist, *Phys. Rev. B* **43,** 1046 (1991).
2. R. D. Shannon, D. B. Rogers, and C. T. Prewitt, *Inorg. Chem.* **10,** 713 (1971).
3. C. T. Prewitt, R. D. Shannon, and D. B Rogers, *Inorg. Chem.* **10,** 719 (1971).
4. S. Okamoto, S. I. Okamato, and T. Ito, *Acta Crystallogr. Sect. B* **28,** 1774 (1972).
5. H. Haas and E. Kordes, *Z. Kristallogr.* **129,** 259 (1969).
6. T. Ishiguro, N. Ishizawa, N. Mizutani, and M. Kato, *J. Solid State Chem.* **49,** 232 (1983).
7. J.-P. Doumerc, A. Ammar, A. Wichainchai, M. Pouchard, and P. Hagenmuller, *J. Phys. Chem. Solids* **48,** 37 (1987).
8. R. J. Cava, A. W. Hewat, E. A. Hewat, B. Batlogg, M. Marezio, K. M. Rabe, J. J. Krajewski, W. F. Peck, Jr., and L. W. Rupp, Jr., *Physica C* **165,** 419 (1990).
9. A. P. Ramirez, *J. Appl. Phys.* **70,** 5952 (1991).
10. C. T. Chen, *Nucl. Instrum. Methods Phys. Res. Sect. A* **256,** 595 (1987); C. T. Chen and F. Sette, *Rev. Sci. Instrum.* **60,** 1616 (1989).
11. L. H. Tjeng, C. T. Chen, and S-W. Cheong, *Phys. Rev. B* **45,** 8205 (1992).
12. C. T. Chen, F. Sette, Y. Ma, M. S. Hybertsen, E. B. Stechel, W. M. C. Foulkes, M. Schluter, S-W. Cheong, A. S. Cooper, L. W. Rupp Jr., B. Batlogg, Y. L. Soo, Z. H. Ming, A. Krol, and Y. H. Kao, *Phys. Rev. Lett.* **66,** 104 (1991).
13. C. T. Chen, L. H. Tjeng, J. Kwo, H. L. Kao, P. Rudolf, F. Sette, and R. M. Fleming, *Phys. Rev. Lett.* **68,** 2543 (1992).